Spin Superlattice Behavior in ZnSe/$Zn_{0.99}Fe_{0.01}Se$ Quantum Wells

W. C. Chou and A. Petrou
Department of Physics and Astronomy and Center for Electronic and Electro-optic Materials, State University of New York at Buffalo, Buffalo, New York 14260

J. Warnock
IBM Research Division, Thomas J. Watson Research Center, Yorktown Heights, New York 10598

B. T. Jonker
Naval Research Laboratory, Washington, D.C. 20375-5000
(Received 15 August 1991)

Spin superlattices with alternating nonmagnetic and magnetic layers, in which a tunable spin-dependent potential exists, have been fabricated. We show that the ZnSe/$Zn_{0.99}Fe_{0.01}Se$ system, in which field-induced spin splitting in both valence and conduction bands can become much larger than the residual zero-field potentials, exhibits spin superlattice behavior. Low-temperature magnetoreflectance experiments have been used to investigate the nature of these structures, verifying through field-dependent spin splittings and transition strengths that they are in fact true spin superlattices.

PACS numbers: 71.35.+z, 73.20.Dx, 78.65.Fa

The incorporation of diluted-magnetic-semiconductor (DMS) layers in quantum-well structures has marked a new era in the study of quantum confinement in semiconductor systems. It has become possible to tune the electronic bands and confining potentials through the application of an external magnetic field [1–3], as a result of the very large effective g factors associated with DMS at low temperatures. These materials offer a unique opportunity to probe the effects of carrier confinement in a system where the quantum-well confining potential can be tuned in a continuous way. Recent magneto-optical studies of ZnSe/$Zn_{1-x}Fe_xSe$ [4] and ZnSe/$Zn_{1-x}Mn_xSe$ [5] quantum wells with $x \simeq 0.1$ have revealed that the confinement of the heavy holes ($m_j = \pm \frac{3}{2}$) can be completely controlled by an externally applied magnetic field, since the zero-field valence-band offset is small and easily overwhelmed by the field-induced spin splitting. However, these systems do not represent true spin superlattices [1] since the zero-field conduction-band offset is relatively large and is only perturbed in a minor way by the magnetic field.

In this work we describe the first observation of a true spin superlattice, where the residual or zero-field quantum-well potentials are small and an external magnetic field controls the spatial localization of both electrons and holes. Strongly asymmetric field-induced spin splittings show that the confining potential is directly dependent on the carrier spin state. In addition, approximately equal excitonic spin component intensities reveal that both electron and hole wave functions are spatially separated according to spin state, a signature of a true spin superlattice. Analysis of the experimental data has been carried out based on calculations of exciton wave functions as the shallow confining potential is varied. These results provide a detailed description of the band splittings and field-induced offsets in these spin superlattice systems.

The spin-superlattice samples investigated here consist of ZnSe/$Zn_{0.99}Fe_{0.01}Se$ layers where the Fe concentration is small enough that the band gaps of ZnSe and $Zn_{0.99}Fe_{0.01}Se$ layers are practically the same. Two spin superlattice structures were studied; sample 1 is a single quantum well, while sample 3 is a multiple-quantum-well structure. In addition, we studied a single $Zn_{0.99}Fe_{0.01}Se$ epilayer in order to measure independently the band splittings of the DMS layers. For comparison, we include in this Letter an $x = 0.1$ ZnSe/$Zn_{1-x}Fe_xSe$ single quantum well (sample 2) with the same dimensions as sample 1. The magneto-optical properties of sample 2 were investigated earlier [4]. In Table I some relevant parameters of the samples used in this work are summarized.

The samples were grown by molecular-beam epitaxy from elemental Knudsen-cell-style sources of Zn, Se, and

TABLE I. Sample parameters. SQW and MQW denote single and multiple quantum wells, respectively.

Sample	DMS layer iron concentration	Layer thickness (Å) DMS layer	ZnSe layer	DMS layer	Type
1	0.01	100	100	100	SQW
2	0.1	100	100	100	SQW
3	0.01	96	96	96	MQW (four periods)
4	0.01	1330	...	...	Epilayer

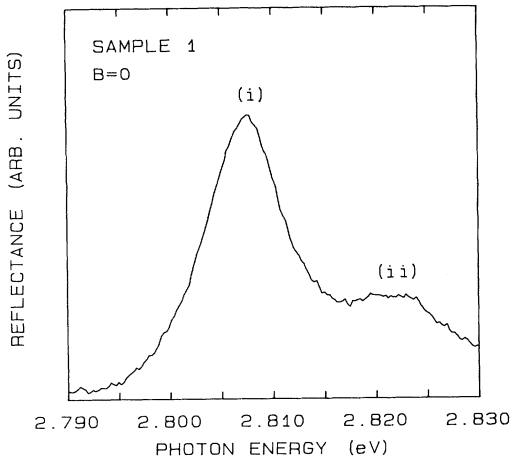

FIG. 1. Zero-field reflectance spectrum at $T=4.2$ K from sample 1. The exciton energies are taken at the maximum of the reflectance energy derivative, 2.803 eV for feature (i) and 2.819 eV for feature (ii), respectively.

Fe on GaAs(001) semi-insulating device-grade wafers. The substrate surface exhibited a well-ordered 4×3 reconstruction as observed by reflection high-energy electron diffraction (RHEED) with the shuttered Se source at operating temperature. All samples were grown in (001) orientation at a substrate temperature of 300 °C and growth rates of 20–40 Å/min, with a Se:Zn beam equivalent pressure ratio $>2:1$. RHEED was used to monitor the growth, and showed a well-ordered Se-stabilized 2×1 surface reconstruction. The thickness and composition of the samples were confirmed by x-ray fluorescence following growth.

The magnetic spin splitting of the excitons was studied using magnetoreflectance spectroscopy in the Faraday geometry in an 8-T superconducting optical magnet cryostat. A monochromatic beam was produced by the combination of a broadband tungsten-halogen lamp and a grating spectrometer. The incident light beam was circularly polarized as either σ_+ or σ_-. The intensity of the reflected beam was synchronously detected by a photomultiplier tube.

In Fig. 1, the zero-field reflectance spectrum from sample 1 is shown. It contains two features marked (i) and (ii) which are attributed to the heavy- and light-hole excitons, respectively. Their degeneracy has been lifted by the presence of in-plane compressive strain due to the lattice mismatch between the GaAs substrate and the ZnSe and ZnFeSe layers [4]. Similar spectra were obtained from the other samples used in this work. In Fig. 2 we plot the energy of the two spin components of the $m_j=\pm\frac{3}{2}$ heavy-hole exciton for sample 1 as a function of magnetic field. The lower $(-\frac{3}{2},-\frac{1}{2})$ component (incident beam σ_+) shows a large redshift with increasing field characteristic of DMS materials. The upper $(+\frac{3}{2},+\frac{1}{2})$ spin component observed in the σ_- polarization shows an initial blueshift with magnetic field; but for

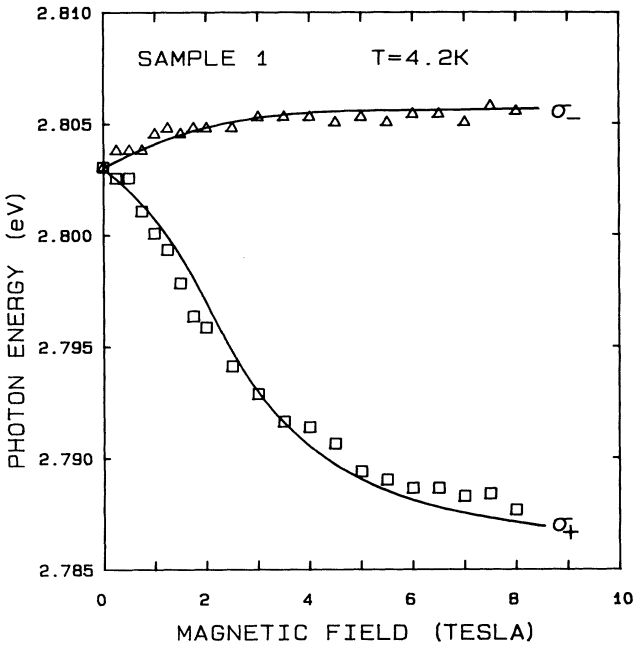

FIG. 2. Energy of the heavy-hole exciton spin components of sample 1 plotted vs magnetic field. Squares, $(-\frac{3}{2},-\frac{1}{2})$ σ_+ transition; triangles, $(+\frac{3}{2},+\frac{1}{2})$ σ_- transition.

$B>3$ T, its energy does not change any more with magnetic field, i.e., it exhibits a nonmagnetic behavior. The dependence of the excitonic spin component energy on magnetic field for sample 1 is quite similar to that of sample 2 which has the same dimensions as sample 1 but much higher Fe concentration. On the other hand, the two structures exhibit different magnetic-field dependence of the intensity ratio $I(+)/I(-)$ between the σ_+ $(-\frac{3}{2},-\frac{1}{2})$ and σ_- $(+\frac{3}{2},+\frac{1}{2})$ heavy-hole-exciton components. In Fig. 3 this ratio is plotted as a function of magnetic field for samples 1 (triangles) and 2 (squares). For sample 2, the ratio drops monotonically with increasing magnetic field, and saturates at $\simeq 0.18$. The ratio $I(+)/I(-)$ has a totally different field dependence for sample 1. After an initial small increase with field it saturates at a value very close to unity and it never exhibits the dramatic decrease with magnetic field which is characteristic of all the $x=0.1$ quantum wells we studied [4]. The solid line in Fig. 3 represents a theoretical fit to the data which is discussed later. A similar dependence of the $I(+)/I(-)$ ratio on magnetic field was observed for the other $x=0.01$ strucutre (sample 3). The magnetic-field dependence of the energy and the intensity of the heavy-hole-exciton spin components for sample 1 can be understood with the help of Fig. 4. In the upper part of Fig. 4 the band alignment at $B=0$ and 8 T is shown schematically. The electron and hole calculated wave functions are plotted in the lower part of this figure. At zero field the band-gap difference between ZnSe and $Zn_{0.99}Fe_{0.01}Se$ is practically zero. When magnetic field is

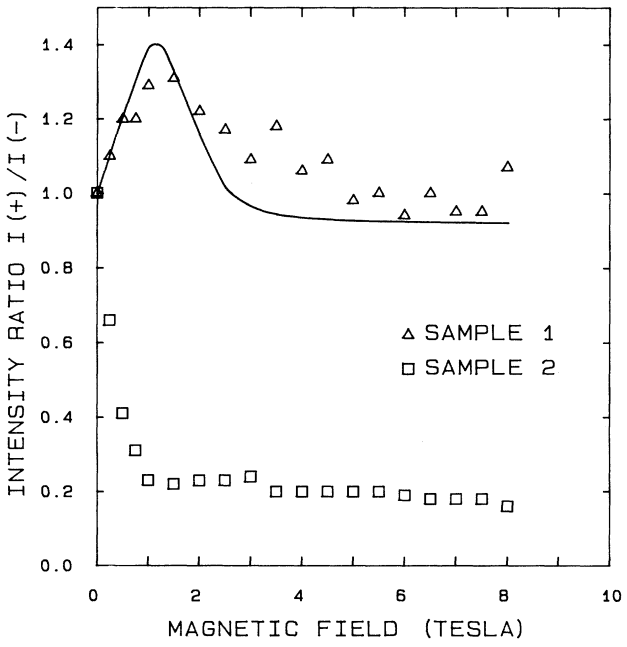

FIG. 3. Intensity ratio $I(+)/I(-)$ of the $(-\frac{3}{2},-\frac{1}{2})$ σ_+ and $(+\frac{3}{2},+\frac{1}{2})$ σ_- heavy-hole exciton components plotted vs magnetic field. Triangles, sample 1; squares, sample 2.

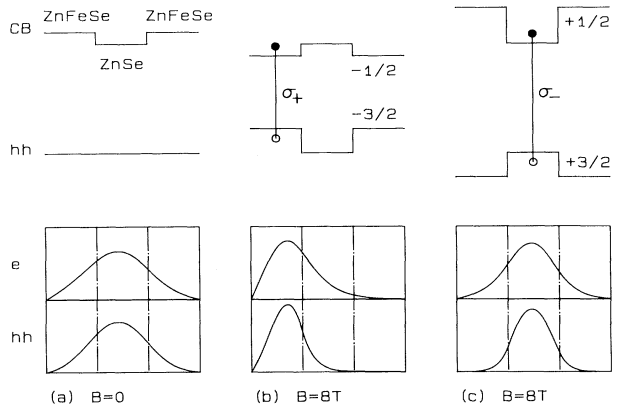

FIG. 4. Upper: Schematic diagram of the band alignment of a $Zn_{0.99}Fe_{0.01}Se/ZnSe/Zn_{0.99}Fe_{0.01}Se$ quantum well. The zero-field conduction-band offset is greatly exaggerated for the sake of clarity. Lower: Calculated electron and heavy-hole wave functions for sample 1, plotted vs distance along the growth direction. (a) $B=0$. (b) $B=8$ T, $m=-\frac{1}{2}$ electrons, $m=-\frac{3}{2}$ heavy holes. (c) $B=8$ T, $m=+\frac{1}{2}$ electrons, $m=+\frac{3}{2}$ heavy holes.

applied the conduction- and valence-band edges of the DMS layers will move as shown in Figs. 4(b) and 4(c). In contrast, the band edges of the nonmagnetic ZnSe layer have a negligible dependence on magnetic field. As a result of the magnetic-field-induced band splittings in the DMS material, the $m_j=-\frac{1}{2}$ electrons and the $m_j=-\frac{3}{2}$ holes are confined in the ZnFeSe layers [Fig. 4(b)], while the $m_j=+\frac{1}{2}$ electrons and the $m_j=+\frac{3}{2}$ holes are located in the nonmagnetic ZnSe layers [Fig. 4(c)]. The two heavy-hole excitonic components become spatially separated in the sense that the σ_+ $(-\frac{3}{2},-\frac{1}{2})$ and the σ_- $(+\frac{3}{2},+\frac{1}{2})$ transitions take place inside the ZnFeSe and ZnSe layers, respectively. Both transitions shown in Figs. 4(b) and 4(c) are type I, i.e., spatially direct. The band diagram shown in Fig. 4 explains the energy dependence of the exciton spin components on magnetic field shown in Fig. 2. The σ_+ transition being confined mostly inside the ZnFeSe layers exhibits a large redshift as a function of magnetic field. On the other hand, the σ_- component taking place mostly inside the ZnSe layer shows nonmagnetic behavior. Since both transitions are type I for $B\neq 0$, their intensities are approximately equal, and thus the ratio $I(+)/I(-)$ is $\simeq 1$. This, along with the asymmetric spin splitting, is a signature of the true spin superlattice and is different from the behavior observed in previous studies of DMS superlattices and quantum wells. In sample 2, the σ_+ transition becomes indirect (type II) and its intensity falls with increasing magnetic field since both $m_j=+\frac{1}{2}$ and $m_j=-\frac{1}{2}$ electrons remain confined in the ZnSe layers even at high-field values; this sample does not behave like a spin superlattice.

To understand quantitatively the phenomena described above, a numerical method was used to calculate exciton wave functions and energies in a quantum-well system with variable confinement. The calculation will only be outlined here, with a detailed description to be presented elsewhere. To calculate the excitonic energy and wave function in a shallow quantum well, we start with an effective Hamiltonian including the quantum-well potential, the electron-hole Coulomb interaction, and the kinetic energies of the electron and hole, and assume a trial variational wave function of the form [6]

$$\psi(r,z_e,z_h)=\psi_e(z_e)\psi_h(z_h)\phi_{e\text{-}h}(r)\,, \tag{1}$$

where ψ_e and ψ_h satisfy the boundary conditions on the separate electron and hole wave functions imposed by the quantum well or periodic superlattice potential, and $\phi_{e\text{-}h}$ describes the relative electron-hole correlation with r the distance from electron to hole. For $\phi_{e\text{-}h}$ the following spherical form was used in our calculation:

$$\phi_{e\text{-}h}(r)\propto\exp(-r/\lambda)\,, \tag{2}$$

with λ a variational parameter. As already discussed in previous work [7] ψ_e and ψ_h cannot be simply chosen as the single-particle solutions to the given quantum-well potential in the limit where the wells are shallow. In the treatment used here these wave functions are obtained by an iterative numerical method. For a given λ, and fixed electron wave function, the hole will experience a potential which is the sum of the quantum-well potential and a Coulomb potential determined from the electron wave function. For this effective potential, the exciton wave function ψ is calculated numerically. Then, the electron

wave function ψ_e is recalculated based on the new hole wave function ψ_h. This procedure is repeated iteratively until self-consistent electron and hole wave functions are obtained. In this way, ψ_e and ψ_h are chosen so that the exciton energy is minimized for a given λ, provided certain convergence criteria are met. The overall minimum energy is then obtained by minimization with respect to λ (recalculating ψ_e and ψ_h as λ is varied). The advantage of this procedure with respect to simpler schemes is that it will provide an accurate solution in the limit of small or negative (type-II) valence- or conduction-band offsets, an essential requirement for treating the spin superlattice.

The fit shown in Fig. 2 (solid lines) was based on the calculation described above, assuming that the $B=0$ valence-band offset is equal to zero. The initial conduction-band offset (3.3 meV) was calculated based on strain-induced effects, and the natural band-gap difference between ZnSe and $Zn_{0.99}Fe_{0.01}Se$. The field-induced band splitting is determined from a $Zn_{0.99}Fe_{0.01}Se$ epilayer, with the ratio between valence- and conduction-band splittings taken from previous work [8]. The data are well described by the calculation, indicating that zero-field valence- and conduction-band offsets are indeed small compared to the field-induced spin splittings. The wave functions obtained from the calculation are shown in the lower part of Fig. 4, and illustrate how the spin states are spatially separated in both the valence and conduction bands. With the calculated wave functions, the transition strengths for the two polarization components can also be calculated. The calculated ratio $I(+)/I(-)$ is shown by the solid line in Fig. 3. The calculation predicts the slight rise in the strength of the σ_+ with respect to the σ_- component at low fields which is observed in the experimental data. At zero field the hole tends to be localized by the Coulomb interaction to a region closer to the center of the quantum well, while the electron wave function spans the whole structure as shown in Fig. 4. As the field is increased, the $m_j = -\frac{3}{2}$ heavy-hole wave function spreads outwards into the magnetic barrier layers, initially increasing the electron-hole wave-function overlap. However, at higher fields, the hole becomes completely localized in the DMS layers, and the overlap decreases as this happens. For the $m_j = +\frac{3}{2}$ heavy hole, the confinement increases with field, much more so than for the electron, causing a slow decrease in the transition strength with field. The analysis of both the field-dependent intensity and exciton energy spin splitting thus confirms the fact that these $ZnSe/Zn_{0.99}Fe_{0.01}Se$ structures are indeed true spin superlattices. Similar effects have been observed recently in ZnSe/ZnMnSe quantum-well structures [9].

In summary, the existence of a new class of superlattice systems has been determined. Magnetoreflectance measurements have confirmed that the structures behave as predicted [1], with important differences from conventional DMS superlattice structures where the magnetic effects on the confining potentials tend to be hidden behind the large built-in zero-field offsets. In the spin superlattice, on the other hand, both conduction and valence bands have near-zero offset at zero field. The large spin splittings in these DMS materials is used to turn on the quantum potentials in a continuous way, allowing observation of the transition into the regime of quantum confinement.

We thank B. D. McCombe, T. Schmiedel, and L. P. Fu for helpful discussions. The work at SUNY was supported by ONR/SDIO under the MMFEL program and NSF, Grant No. DMR8922177; at NRL work was supported by the Office of Naval Research.

[1] M. von Ortenberg, Phys. Rev. Lett. **49**, 1041 (1982).
[2] S. Datta, J. K. Furdyna, and R. L. Gunshor, Superlattices Microstruc. **1**, 327 (1985).
[3] J. A. Brum, G. Bastard, and M. Voos, Solid State Commun. **59**, 561 (1986).
[4] X. Liu, A. Petrou, J. Warnock, B. T. Jonker, G. A. Prinz, and J. J. Krebs, Phys. Rev. Lett. **63**, 2280 (1989).
[5] X. C. Liu, W. C. Chou, A. Petrou, J. Warnock, B. T. Jonker, G. A. Prinz, and J. J. Krebs, in *Proceedings of the Twentieth International Conference on the Physics of Semiconductors,* edited by E. M. Anastassakis and J. D. Joannopoulos (World Scientific, Singapore, 1990), pp. 621–624.
[6] G. Bastard, E E. Mendez, L. L. Chang, and L. Esaki, Phys. Rev. B **26**, 1974 (1982).
[7] S. K. Chang, A. V. Nurmikko, J. W. Wu, L. A. Kolodziejski, and R. L. Gunshor, Phys. Rev. B **37**, 1191 (1988).
[8] X. Liu, A. Petrou, B. T. Jonker, G. A. Prinz, J. J. Krebs, and J. Warnock, Appl. Phys. Lett. **53**, 476 (1988).
[9] N. Samarth (private communication).